



**HAL**  
open science

## Microfluidic Device for the Crystallization of Organic Molecules in Organic Solvents.

Sébastien Teychené, Béatrice Biscans

► **To cite this version:**

Sébastien Teychené, Béatrice Biscans. Microfluidic Device for the Crystallization of Organic Molecules in Organic Solvents.. *Crystal Growth & Design*, 2011, 11 (11), pp.4810-4818. 10.1021/CG2004535 . hal-03469375

**HAL Id: hal-03469375**

**<https://hal.science/hal-03469375>**

Submitted on 7 Dec 2021

**HAL** is a multi-disciplinary open access archive for the deposit and dissemination of scientific research documents, whether they are published or not. The documents may come from teaching and research institutions in France or abroad, or from public or private research centers.

L'archive ouverte pluridisciplinaire **HAL**, est destinée au dépôt et à la diffusion de documents scientifiques de niveau recherche, publiés ou non, émanant des établissements d'enseignement et de recherche français ou étrangers, des laboratoires publics ou privés.



## Open Archive Toulouse Archive Ouverte (OATAO)

OATAO is an open access repository that collects the work of Toulouse researchers and makes it freely available over the web where possible.

This is an author-deposited version published in: <http://oatao.univ-toulouse.fr/>  
Eprints ID: 6042

**To link to this article:** DOI:10.1021/CG2004535  
URL: <http://dx.doi.org/10.1021/CG2004535>

**To cite this version:** Teychené, Sébastien and Biscans, Béatrice (2011) Microfluidic Device for the Crystallization of Organic Molecules in Organic Solvents. *Crystal Growth & Design*, vol. 11 (n°11). pp. 4810-4818. ISSN 1528-7483

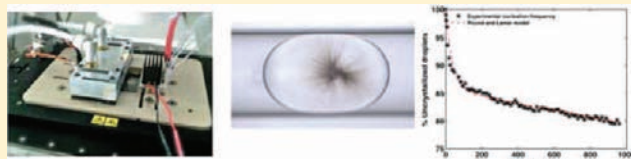
Any correspondence concerning this service should be sent to the repository administrator: [staff-oatao@listes.diff.inp-toulouse.fr](mailto:staff-oatao@listes.diff.inp-toulouse.fr)

# Microfluidic Device for the Crystallization of Organic Molecules in Organic Solvents

Sébastien Teychené\* and Béatrice Biscans

Laboratoire de Génie Chimique, UMR CNRS 5503, Université de Toulouse, 4 Allée Emile Monso, 31432 Toulouse, France

**ABSTRACT:** A microfluidic chip suitable for studying crystallization of organic molecules in organic solvents was developed. In this device, supersaturation can be generated either by thermal gradient (i.e., when the crystallization solvent is not miscible with the continuous phase) or by mass transfer (when the crystallization solvent is partially miscible with the continuous phase) or both. The experimental setup allows the storage of up to 2000 droplets to get nucleation statistics and crystal growth rates under static conditions. Crystallization of efflumibe in droplets of octanol generated in water was investigated by use of this experimental device. The results show that, at lower time scale, the first nucleation events result mainly from a heterogeneous nucleation process (due to the presence of impurities or to the octanol–water interface itself). At higher time scales, the nucleation rate falls off, all the crystals appear in the droplet volume, and nucleation becomes homogeneous. This microfluidic device allows heterogeneous and homogeneous nucleation rate measurements to be performed in a single experiment. For ibuprofen crystallization in organic solvents partially miscible with water, no crystallization was observed, even at high time scales. Instead of crystallizing, the system undergoes a liquid–liquid phase separation. The liquid–liquid system obtained has a long lifetime, and contrary to what is usually observed, this metastable state does not promote nucleation of stable crystals.



## INTRODUCTION

Crystallization from solution is a core technology for purification, separation, and control of pharmaceuticals, pigments, and other specialty compounds. When designing an industrial crystallization process, engineers usually focus on the determination of fundamental data such as liquid–solid equilibrium (solubility), nucleation, and crystal growth kinetic and phase transitions (liquid–liquid phase separation and polymorphism). Despite many experimental and theoretical developments, crystallization remains a puzzling phenomenon, coupling several complex mechanisms, and empirical approaches are still needed. However, in the early development stage of a new product, for instance, in the pharmaceutical industry, very low amounts of product are available, leading to a limited number of experiments and thus to a poor understanding of the whole crystallization process. Because nucleation is the initiation of the liquid–solid phase transition, it is one of the most critical phenomena of the crystallization process. As it is a stochastic phenomenon, numerous identical experiments are needed with a small amount of product to determine precisely the nucleation mechanism and the associated kinetics.

The pioneering work of Turnbull and Vonnegut<sup>1</sup> and Pound and La Mer<sup>2</sup> on crystal nucleation kinetics of molten alloy and water droplets has inspired numerous actual experimental techniques such as levitated droplets<sup>3</sup> and hanging or sitting drops. Droplet microfluidic is the most recent technique and has shown great potential for storing processing and controlling fluids and molecules in time and space. For the first time, Ismagilov and co-workers have developed high-throughput microfluidic

platforms<sup>4–6</sup> for the identification of optimal conditions to produce high-quality protein crystals for X-ray and neutron crystallography. Microfluidic crystallization systems have also enabled the measurement of nucleation kinetics, solubility profiles, and polymorphic transitions of inorganic salts ( $\text{KNO}_3$ )<sup>8,9</sup> and small organic molecules ( $\alpha$ -lactose),<sup>10</sup> with a few micrograms of starting materials. More recently, a stochastic model was formulated<sup>11</sup> for crystal nucleation in droplet-based microfluidic systems to any form of nucleation rate expression under condition of time-varying supersaturation. The analytical solution describes evolution of the probability of crystal nucleation, average number of crystals in a droplet, and induction time statistics.

However, most of the aforementioned studies use poly(dimethylsiloxane) (PDMS) for building the microfluidic chip. PDMS is known to have poor solvent compatibility,<sup>7</sup> and organic solvents, frequently encountered in the fine chemical or pharmaceutical industry, usually swell PDMS. This swelling induces modification of droplet volume and diffusion of solvent or organic molecules in the chip. So previous studies were restricted to the use of water as the crystallization solvent. Until now, there has been no study dealing with the crystallization of organic molecules in organic solvents. This paper focus on the design and the use of a glass microfluidic chip for the crystallization of organic molecules in organic solvents. First, thermodynamic and kinetic considerations used for the chip design are presented.

**Table 1. Physicochemical Properties of Ethanol and Eflucimibe Solution at 293 K**

	ethanol	eflucimibe
$v_i$ (cm <sup>3</sup> ·mol <sup>-1</sup> )	40.50	4800.00
$M$ (g·mol <sup>-1</sup> )	46.07	469.73
$10^4 x_{\text{eflu}}^{\text{sat}}$		5.00
$\sigma$ (mJ·m <sup>-2</sup> )		2.50

Then the crystallization of two organic molecules is taken as an example, and the results obtained in terms of nucleation, crystal growth, and phase transition (liquid–liquid phase separation) are presented and discussed.

## DESIGN OF MICROFLUIDIC CRYSTALLIZER

**Thermodynamic and Kinetic Considerations.** One hypothesis of classical nucleation theory (CNT) is the infinite size of the system: supersaturation is considered to be constant all along the emergence of an “ $n$ -sized cluster” (no change in the Gibbs free energy of the parent phase). In microfluidic devices, the system is shrunk down to nanometer or micrometer scales, and in some cases (large molecules, very low solubility), it cannot be considered as infinite. From a thermodynamic point of view, to be representative of a classical crystallization process, the size of the microchannels, and thus the droplet size, has to be precisely designed to consider the system as infinite. Under constant pressure and temperature conditions, and with the assumption that a spherical nucleus is formed (with an area of  $4\pi r^2$ ), the classical nucleation theory describes the Gibbs free energy change during homogeneous nucleation as

$$\Delta G_{\text{nucl}}^{\text{conf}} = 4\pi r^2 \sigma - \frac{4\pi r^3}{3v_A} RT \ln S_{\text{ini}} \quad (1)$$

where  $v_A$  is the molar volume of pure component A in the liquid state,  $r$  is the radius of the spherical nucleus,  $R$  is the gas constant,  $T$  is the absolute temperature,  $\sigma$  is the interfacial tension between the nucleus and the parent phase, and  $S_{\text{ini}} = n_A^{\text{ini}}/(x_A^{\text{sat}} n_T)$  is the initial supersaturation. This equation is derived from the assumption of unchanged free energy in the parent phase during the nucleation process. Once a critical nucleus is formed [with a critical radius that corresponds to the maximum of the  $\Delta G_{\text{nucl}} = f(r)$  curve], it grows until the solution reaches the thermodynamic equilibrium.

In confined systems (i.e., in a very small crystallization container), when a molecule leaves the solution to form a nucleus, the chemical potential of the solution (i.e., those of the solute and of the solvent) cannot be considered constant anymore. To take into account the evolution of Gibbs free energy change due to the emergence of a nucleus in a confined system, several authors<sup>12–14</sup> have proposed a modification of eq 1. Following the formalism of Wasai et al.,<sup>12</sup> the CNT equation may be rewritten as follows:

$$\begin{aligned} \Delta G_{\text{nucl}}^{\text{conf}} &= G - G_{\text{ini}} \\ &= \sum_{i=1}^c n_i^n (\mu_i^n - \mu_i^{\text{sol}}) + \sum_{i=1}^c n_i^{\text{ini}} (\mu_i^{\text{sol}} - \mu_i^{\text{ini}}) \\ &\quad + \sum_{i=1}^c n_i^{\text{int}} (\mu_i^{\text{int}} - \mu_i^{\text{sol}}) + \sigma A \end{aligned} \quad (2)$$

where  $\mu_i$  and  $n_i$  are the chemical potential and mole number of component  $i$ , respectively. The superscripts sol, n, int, and ini indicate solution (parent phase), nucleus, interfacial phase, and initial solution respectively. Further details on the development and validity of eq 2 can be found in the paper of Wasai et al.<sup>12</sup>

For the nucleation of a unique solid nucleus composed of a single component (A) from  $n_T$  moles of a binary solution (solute A and solvent B), with the assumption of  $\sum n_i^{\text{int}} (\mu_i^{\text{int}} - \mu_i^{\text{sol}}) \approx 0$ , the Gibbs free energy change during the nucleation process in a confined system may be written as follows:

$$\Delta G_{\text{nucl}}^{\text{conf}} = 4\pi r^2 \sigma - n_A^n RT \ln \frac{a_A^{\text{sol}}}{a_A^{\text{sat}}} + n_A^{\text{ini}} RT \ln \frac{a_A^{\text{sol}}}{a_A^{\text{ini}}} + n_B^{\text{ini}} RT \ln \frac{a_B^{\text{sol}}}{a_B^{\text{ini}}} \quad (3)$$

In the case of an ideal solution, each activity coefficient equals the mole fraction:

$$a_i^{\text{ini}} = x_i^{\text{ini}} = \frac{n_i^{\text{ini}}}{n_T} \quad (4a)$$

$$a_A^{\text{sol}} = x_A^{\text{sol}} = \frac{n_A^{\text{ini}} - n_A^n}{n_T - n_A^n} \quad (4b)$$

$$a_B^{\text{sol}} = x_B^{\text{sol}} = \frac{n_B^{\text{ini}}}{n_T - n_A^n} \quad (4c)$$

$$n_T = (n_A^{\text{sol}} + n_A^n) + n_B^{\text{ini}} = n_A^{\text{ini}} + n_B^{\text{ini}} \quad (4d)$$

which simplifies eq 3 to

$$\begin{aligned} \Delta G_{\text{nucl}}^{\text{conf}} &= 4\pi r^2 \sigma - n_A^n RT \ln S_{\text{ini}} + (n_A^{\text{ini}} - n_A^n) RT \ln \left( \frac{1 - n_A^n/n_A^{\text{ini}}}{1 - n_A^n/n_T} \right) \\ &\quad + (n_T - n_A^{\text{ini}}) RT \ln \left( \frac{1}{1 - n_A^n/n_T} \right) \end{aligned} \quad (5)$$

To check the impact of confinement on nucleation of real systems, the model was applied to small droplets (from a few picoliters to a few nanoliters) containing a pharmaceutical ingredient (eflucimibe, C<sub>29</sub>H<sub>43</sub>NO<sub>2</sub>S) and ethanol. The physicochemical properties of the solution, used as input data for the model, are given in Table 1.

The evolution of  $\Delta G_{\text{nucl}}^{\text{conf}}$  and  $\Delta G_{\text{nucl}}^{\text{conf}}$  obtained for droplet volumes ranging from 1 pL to 20 nL and for an initial supersaturation of  $S_{\text{ini}} = 1.4$  was calculated and is shown in Figure 1a. As the supersaturation ratio is not constant during the nucleation process, the evolution of the Gibbs free energy is also plotted versus a nondimensional supersaturation ratio in Figure 1b. This supersaturation ratio is calculated as

$$S_{\text{conf}} = \frac{n_A^{\text{sol}}}{n_A^{\text{sat}}} = \frac{n_A^{\text{ini}} - n_A^n}{n_A^{\text{sat}}} \quad (6)$$

The figure shows that a local minimum of the Gibbs free energy is obtained for a droplet diameter lower than 2  $\mu\text{m}$ . Once the critical nucleus is formed, it will grow and stop growing when the local minimum is attained, even if the solution is not at the thermodynamic equilibrium ( $x_{\text{sol}} > x_{\text{sat}}$ ). For instance, for a 500 nm drop diameter, the local minimum is obtained for a supersaturation ratio of 1.2. As stated by Wasai et al.,<sup>12</sup> the minimum in nucleation processes from a supersaturated parent phase would provide a theoretical possibility to stabilize a nanocrystal. However, these

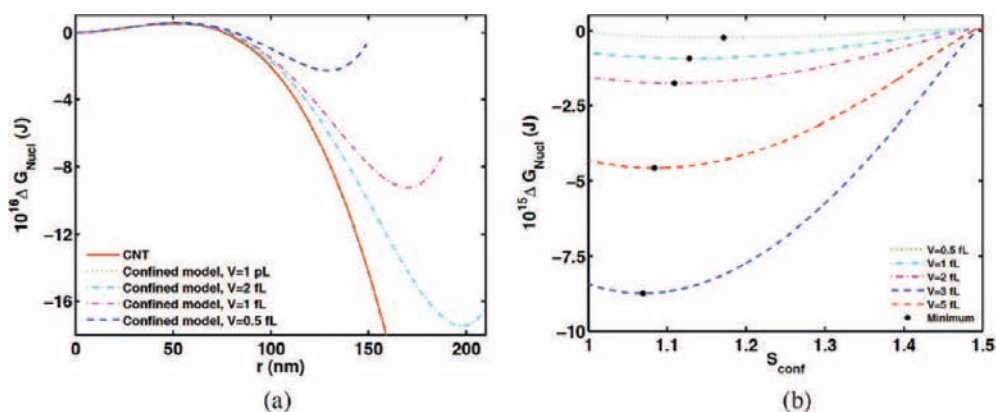


**Figure 1.** Evolution of Gibbs free energy during nucleation in confined system. (a) Comparison between evolution of  $\Delta G_{\text{nucl}}^{\text{conf}}$  and  $\Delta G_{\text{nucl}}^{\infty}$  vs nucleus radius. (b) Evolution of  $\Delta G_{\text{nucl}}^{\text{conf}}$  vs supersaturation (evidence of local minimum for  $x_A > x_{\text{sat}}$ ).

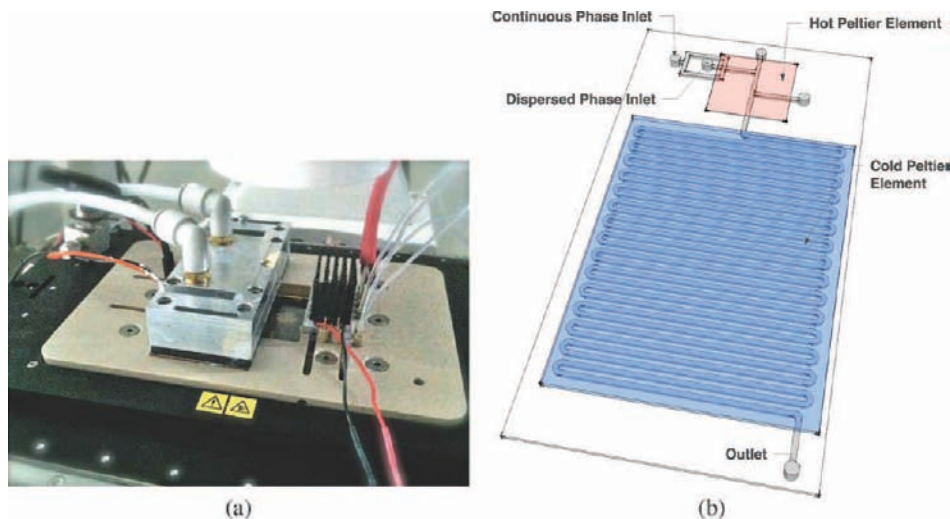


**Figure 2.** Microfluidic crystallization chip: (a) photograph of microfluidic chip and housing; (b) sketch of microfluidic chip.



**Figure 3.** Experimental setup.

results are obtained by a classical thermodynamic approach to nucleation and are valid in the thermodynamic limit, where the

**Table 2. Volumetric Flow Rates and Physicochemical Properties of the Two-Phase Flow of Immiscible Fluids at 293.15 K**

	$Q \text{ (}\mu\text{L}\cdot\text{h}^{-1}\text{)}$	$\rho \text{ (kg}\cdot\text{m}^{-3}\text{)}$	$\mu \text{ (mPa}\cdot\text{s)}$	$\gamma_{i/w} \text{ (mN}\cdot\text{m}^{-1}\text{)}$
water	50–1000	999	1	
octanol	2–1000	805	6.13	8.23
toluene	5–1000	868	0.570	36.1
<i>n</i> -heptane	5–1000	684	0.386	50.9

system is so large that the property fluctuations can be neglected. As the system becomes smaller, the effect of fluctuations can no longer be neglected; they may strongly modify the observed properties and could result in a critical nucleus growing larger than expected by the Gibbs free energy minimum.

When microfluidic devices are used for the determination of nucleation frequencies, the droplet volumes generated in these systems (from a few picoliters to a few nanoliters) are far from the “confinement limit” previously determined (around 2–5 fL). Moreover, eflucimibe is one of the worst cases, because the molecule is large and has very low solubility in the solvent. For most small

organic molecules (ibuprofen, paracetamol, etc.), the effect of confinement is significant for a droplet diameter lower than a few nanometers (i.e., for a volume lower than 0.5 fL). Finally, this approach allows us to state that all the data obtained in classical microfluidic devices are representative, from a thermodynamic point of view, of large-scale crystallization processes.

From a kinetic point of view, a characteristic nucleation time can be considered as the mean time required for one nucleation event to occur in a system of volume  $V$ . If the solution is spatially uniform and nucleation is homogeneous, then, the mean induction time for the appearance of at least one crystal, in a droplet of constant supersaturation and volume, is given by the following equation:<sup>11</sup>

$$t_{\text{ind}} = \int_0^{\infty} J V t \exp(-J V t) dt = \frac{1}{J V} \quad (7)$$

For instance, for strictly identical operating conditions, if the average induction time for the appearance of the first crystal is 10 s in 10 mL of solution, then it will be almost 1 day in a 100  $\mu\text{m}$  drop. This means that in this type of system the limiting step is kinetic, and a higher undercooling level can be reached before the appearance of the first crystal, which allows us to explore more deeply the phase diagram.

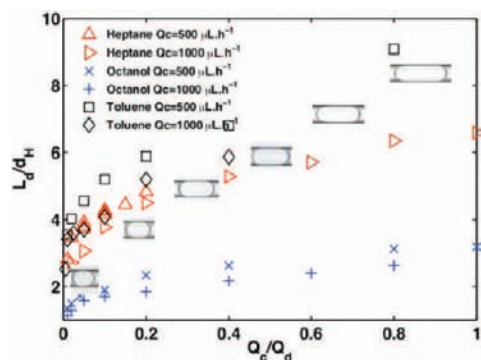


**Figure 4.** Evolution of droplet diameters and morphologies as a function of volumetric flow rate ratio for three different solvents.

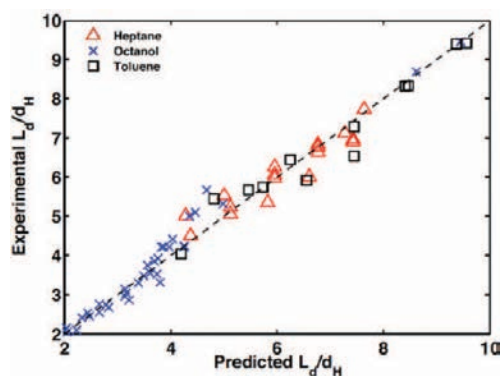


**Figure 5.** Comparison of experimental and predicted droplet lengths of octanol, *n*-heptane, and toluene in water.

## ■ MATERIALS AND METHODS

Organic solvents octan-1-ol, ethyl acetate, methyl ethyl ketone, and *n*-heptane were purchased from Sigma–Aldrich (with a minimum purity of 99.5%). The solvents were used without further purification. Double-distilled water was processed through a Barnstead EASY pure UV system and was used as the continuous phase. The water resistivity was greater than 18 M $\Omega$ ·cm. Ibuprofen ( $\text{C}_{13}\text{H}_{18}\text{O}_2$ ,  $M = 206.2 \text{ g}\cdot\text{mol}^{-1}$ ) was supplied by BASF with a purity greater than 99%. Eflucimibe ( $\text{C}_{29}\text{H}_{43}\text{NO}_2\text{S}$ ,  $M = 469.73 \text{ g}\cdot\text{mol}^{-1}$ ) was supplied by Pierre Fabre Co., Gaillac, France. Its chemical purity, evaluated by high-performance liquid chromatography, was more than 99.5%.

**Experimental Setup.** Microfluidic chips were designed with different materials: poly(dimethylsiloxane) (PDMS), silicon-glass, and glass. PDMS was quickly rejected because of the swelling of the polymer in contact with organic solvents.<sup>7</sup> In addition, silicon-glass microfluidic systems were found to be too weak (due to the syringe to chip connection). Moreover, it was very difficult to impose a temperature gradient on this chip due to the high thermal conductivity of silicon.

A glass microfluidic chip was the best solution for studying crystallization of organic product in organic solvents. Glass is hydrophilic by nature, allowing the generation of organic solvent droplets in water without surfactant. The low thermal conductivity of glass allows us to easily impose a linear temperature gradient across the chip. The glass microfluidic chips were built by Micronit (Enschede, Netherland). The crystallization chip consists of a 2.5 m long channel with  $220 \times 100 \mu\text{m}^2$  cross-sectional dimensions. As shown in Figure 2, the chip is divided into two parts. The first part is used to generate droplets either by flow focusing or by a T junction. Monodispersed droplets (in the 20–110 nL range) are formed at the intersection between the two streams for typical volume flow rates ranging from 500 to 1500 and from 10 to 800  $\mu\text{L}\cdot\text{h}^{-1}$  for the aqueous and organic streams, respectively. This part is thermally controlled by a Peltier module (Melcor,  $10 \times 30 \text{ mm}^2$ ) and a Pt100 sensor placed in a copper plate between the chip and the Peltier module. This part can be heated up to  $50 \pm 0.05 \text{ }^\circ\text{C}$ . The second part of the chip consists of a 2.5 m long serpentine and was designed to reach high enough residence time (up to 20 min) to observe crystallization under flow or to store up to 2000 droplets to get nucleation statistics. The temperature of the serpentine is controlled by a large Peltier module ( $40 \times 40 \text{ mm}^2$ , Melcor) and a Pt100 sensor. This part can be cooled down to  $-10 \text{ }^\circ\text{C}$ . The temperature sensors and the Peltier modules are coupled to a PID regulator (ALI 2420, AMS technologies), allowing control of the chip temperature. Computer automation of the regulator enables application of temperature profiles with cooling/heating rates up to  $0.5 \text{ }^\circ\text{C}\cdot\text{s}^{-1}$  (Matlab). Temperature is also measured at different points in the chip with six platinum microsensors inserted into the chip with a precision of  $\pm 0.02 \text{ }^\circ\text{C}$ . The large size of the Peltier element used yields a uniform temperature field, and the temperature variation is below  $0.05 \text{ }^\circ\text{C}$ .

Glass syringes, equipped with patterned filters (Millipore, pore diameter  $< 0.2 \mu\text{m}$ ), are used to load the fluids into the devices. The temperature of the syringe and the tubing containing the organic solution are also controlled to avoid crystallization by use of a small flexible heater. Flow rates are controlled by syringe pumps (PhD 2000, Harvard apparatus).

The system is observed under a semiautomatic inverted light microscope (Zeiss AXIO pbserved, motorized stage from Ludl Electronic Product) and images are acquired by use of a sensitive charge-coupled device (CCD)

**Table 3.** Volumetric Flow Rates and Physicochemical Properties of the Two-Phase Flow of Partially Miscible Fluids at 293.15 K

	$Q$ ( $\mu\text{L}\cdot\text{h}^{-1}$ )	$\rho$ ( $\text{kg}\cdot\text{m}^{-3}$ )	$\mu$ (mPa·s)	$\gamma_{i/w}$ (mN·m $^{-1}$ )	solubility ( $w^*$ )
water	500–1000	999	1		
ethyl acetate	5–800	897	0.426	6.8	0.087
methyl ethyl ketone	5–800	805	0.43	$\approx 1$	0.27

color camera (PCO Sensicam QE). The optical resolution of the system is 1  $\mu\text{m}/\text{pixel}$  with the 10 $\times$  objective, and the particle detection threshold is around 5  $\mu\text{m}$ . The experimental setup is shown in Figure 3.

## RESULTS AND DISCUSSION

**Microfluidic Experiments. Immiscible Fluid Flow.** Droplets of toluene, n-heptane, and octanol were generated in water (continuous phase). In these cases, as the continuous and dispersed phases are not miscible (i.e., no mass transfer occurs between the continuous and the dispersed phase), the droplet diameter remains constant all along the channel. In a typical experiment, drops of a given size are formed at a given frequency  $f$  and move down the channel at a speed  $U_d$ . The frequency of drop production is measured by direct counting, and the speed is measured by tracking the drop center of mass for a short distance in the channel. The range of operating conditions tested is given in Table 2.

An example of the evolution of droplet diameters and typical morphologies as a function of the volume flow rate ratio for three different solvents is shown in Figure 4.

In all these experiments, a small difference between the speed of the drops and the average velocity of the continuous phase (less than 6%) is expected. In general, the error bars are the symbol size or smaller. From the experiments performed, a correlation was established to predict the droplet diameter, with a precision of  $\pm 10\%$ , as a function of the fluid properties and the volumetric flow rates. The obtained equation is the following:

$$\frac{L_{\text{drop}}}{d_h} = 1.5 \left( \frac{Q_{\text{disp}}}{Q_{\text{cont}}} \right)^{0.2} Ca^{-0.2} \left( \frac{\mu_{\text{disp}}}{\mu_{\text{cont}}} \right)^{-0.2} \left( \frac{\rho_{\text{disp}}}{\rho_{\text{cont}}} \right)^{1/3} \quad (8)$$

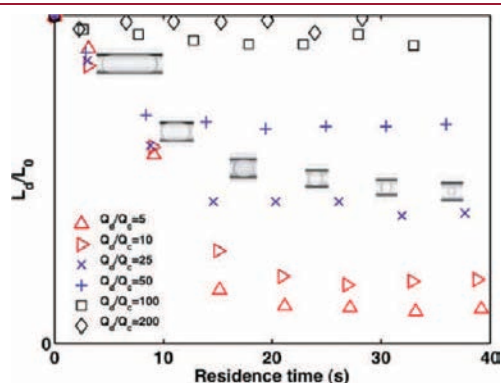


**Figure 6.** Evolution of droplet diameters and morphologies as a function of droplet residence time for different flow rates of ethyl acetate and  $Q_c = 500 \mu\text{L} \cdot \text{h}^{-1}$ .

where  $L_{\text{drop}}$  is the droplet length (in micrometers),  $d_h$  is the hydraulic diameter of the channel, and  $Ca = U_d \mu / \sigma$  is the capillary number. It represents the relative effect of viscous forces versus surface tension acting across an interface. The comparison of predicted and measured droplet lengths is given in Figure 5. These results allow us to generate crystallization containers with a constant volume, without added impurities (surfactant or polymer), and with controlled operating conditions (volume, concentration, and temperature).

**Partially Miscible Fluids.** Organic solvent droplets, when present in a partially miscible continuous phase that has a slight solubility in the organic solvent, will shrink and concentrate their contents via diffusion and dissolution into the continuous phase. In this way, droplets of ethyl acetate and methyl ethyl ketone in water were generated in the microsystem. To follow the evolution of droplet diameters, 10–20 images were taken at different positions in the channel (i.e., at droplet generation, beginning of the serpentine, and end of the serpentine) for each flow rate tested. The range of flow rates tested and the chemical properties of the fluids are given in Table 3. The size of the droplets was automatically measured with a homemade image treatment software written in Matlab. Examples of the evolution of ethyl acetate droplet diameters in water as a function of time are plotted in Figure 6 for different flow rates. In the beginning of the process, there is a rapid decrease of droplet diameter and then it reaches a constant value. The curves flatten out because the external phase is saturated with the organic solvent. Nonetheless, this saturation level is several times lower than the expected equilibrium value. This effect may result from the existence of depleted zones in the external phase. Consequently, the droplet “sees” an average concentration of organic solvent in water higher than the average concentration in the volume, and thus, the saturation level lies below the theoretical value, which assumes homogeneity in the reservoirs. On the basis of these experiments, for a crystallization purpose, and with the assumption that no water enters into the droplet, the initial supersaturation can be directly deduced from evolution of the droplet diameter ( $L_d$ ):

$$S = \frac{C}{C^*} = \frac{V^{\text{initial}}}{V} \approx \frac{L_d^{\text{ini}}}{L_d} \quad (9)$$

**Crystallization Experiments. Eflucimibe Crystallization: Qualitative Observations.** In previous works,<sup>15–17</sup> crystallization of eflucimibe was studied in detail, and it was found to crystallize into two monotropically related polymorphs, identified as A (the stable one) and B. The two polymorphs differ by a conformational change of the phenyl group in the crystal lattice. When the crystallization process is carried out in polar solvents (i.e., alcohol, ketone, etc.), as the volume fraction of the crystal rises

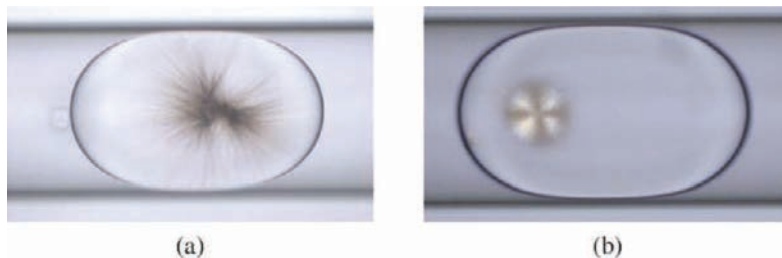


**Figure 7.** Photographs of eflucimibe crystals obtained at (a) 20 and (b) 5  $^{\circ}\text{C}$ .

during cooling, the suspension evolves toward a very structured gel-like network. To characterize the suspension behavior, rheological measurements were performed. It was found that the suspension behaves as a plastic fluid, and for particle concentrations higher than 2%, needlelike growing crystals form a network in which the solvent is trapped. However, at this point, due to the weakness of the crystal formed, it was impossible to characterize the morphology of the crystal responsible of the network formation.<sup>18</sup>

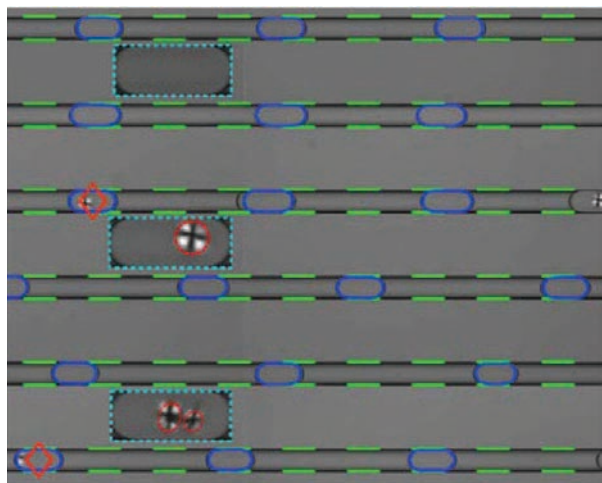


Figure 8. Portion of microfluidic crystallizer with example of droplets and crystal detection.

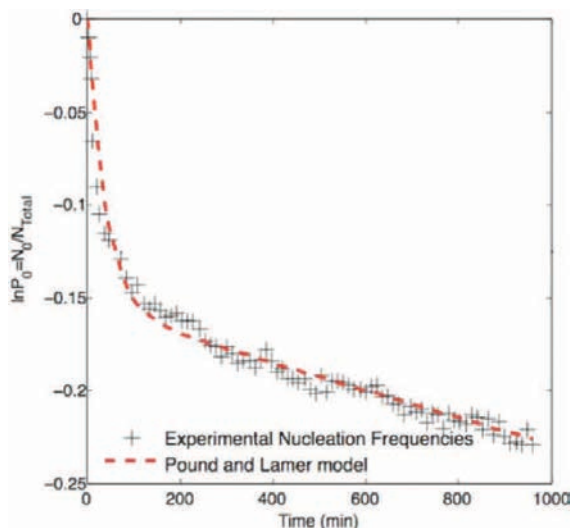


Figure 9. Evolution of proportion of uncrystallized droplets as a function of time.

To study the crystallization of eflocimibe in octanol, up to 2000 droplets were generated at 45 °C with flow rates of 200 and 500  $\mu\text{L}\cdot\text{h}^{-1}$  for octanol and water, respectively. In this experiment, eflocimibe concentration was  $C^* = 13.78 \text{ mg}\cdot\text{g}^{-1}$ , corresponding to its solubility in octanol at 40 °C. Once the droplets are stored, the system is cooled down to either 20 or 5 °C. The solubility of eflocimibe in octanol is  $7.84 \text{ mg}\cdot\text{g}^{-1}$  at 20 °C and  $4.88 \text{ mg}\cdot\text{g}^{-1}$  at 5 °C.

The first crystals were obtained in the droplet for an induction time of 75 min at 20 °C and 45 min at 5 °C. Photographs of the crystals obtained at 20 and 5 °C are given in Figure 7. As shown in Figure 7, the crystals obtained are spherulites. At 20 °C, if the droplet flows in the channel, the branches of the spherulitic crystal (shown in Figure 7a) restrict the flow inside the droplet. These observations, at the micrometric scale, can be related to the rheological behavior of the suspension obtained in a previous study.<sup>18</sup> At 5 °C, as shown in Figure 7b, the crystals obtained are still spherulites but with a denser structure that might be easier to handle in a crystallizer. In that case, if the droplet flows inside the channel, the crystal moves freely inside the droplet. This example clearly shows that microfluidic tools coupled with analytical techniques can be very useful to study, qualitatively and quantitatively, the crystallization process of complex structures under flow at a microscopic scale.

*Eflocimibe Nucleation Experiments.* To determine nucleation kinetics of eflocimibe, the number of crystals appearing is recorded as a function of time. The detection of eflocimibe crystals formed in the droplets is based on their birefringent properties. An image processing program counts automatically the number  $N$  of crystals appearing in each droplet ( $N_1$  for one crystal per drop,  $N_2$  for two crystals per drop, etc.) and the total number  $N_t$  of droplets. For an experiment in which  $N$  events are observed in  $N_t$  trials, the probability to observe one event is  $P_i = N_i/N_t$ . The error in determination of  $P_i$  is given by the standard deviation of the binomial distribution function of  $P$  in the case of independent events. Experimentally,  $P$  is determined from statistics on about 1000 droplets, the results being the same for experiments carried out on 2000 droplets. An example of the droplet counting and crystal detection is given in Figure 8.

During the whole crystallization process, only four droplets contained multiple crystals. The obtained evolution of probability  $P_0$  (probability of finding no crystal in droplet) as a function of time is plotted in Figure 9. Obviously, the probability of finding one crystal in a droplet is  $P_1 = 1 - P_0$ .

As previously shown by several authors,<sup>1,19</sup> nucleation is a stochastic process and the Poisson distribution provides a good fit of the number of crystals nucleated in droplets at constant supersaturation. In microfluidic devices, the solution is spatially uniform and the nucleation events occur independently and not simultaneously from one droplet to another.<sup>10,20</sup> The time evolution of the probability that a droplet does not contain any crystal is then described, at a constant supersaturation and

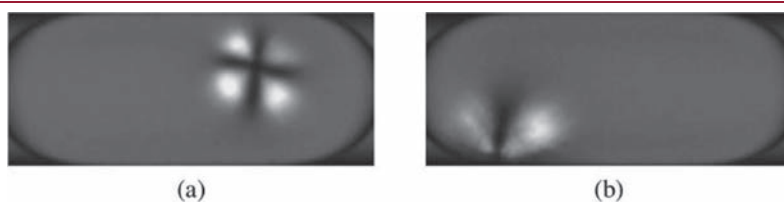


Figure 10. Photograph of eflocimibe crystals obtained (a) in the droplet volume and (b) at the octanol/water interface.

temperature, by the following equation:

$$P_0 = \frac{N_0}{N_t} = \exp(-Jt) \quad (10)$$

For nucleation experiments performed at 20 °C, the obtained evolution of  $\ln P_0$  as a function of time is represented in Figure 9. According to classical nucleation theory, the rate of crystallization should be first-order. However, inspection of the data shows that the logarithm of the number of uncrystallized droplets is not linear with time but exhibits marked curvature with decreasing slope. Figure 9 strongly suggests that nucleation is not homogeneous and cannot be described by a classical Poisson distribution.

Even if the solutions were carefully prepared to avoid the introduction of impurities in the system (dust, solid interfaces, etc.) in the system, it is believed that the formation of crystals in the droplets would be mainly due to a heterogeneous nucleation process. One possible explanation of the lack of linearity in Figure 9 is that most of the crystals nucleated at the octanol–water interface (as shown in Figure 10b). Impurities that catalyze nucleation could be located at the octanol–water interface, or the interface could act as a catalyst for nucleation.

In their work on nucleus formation in supercooled liquid tins, Pound and La Mer<sup>2</sup> described the heterogeneous nucleation process with the assumption that impurities are randomly distributed among the droplets. If the Poisson distribution is applicable to the distribution of impurities among the droplets, the time evolution of the probability that a droplet does not contain a crystal is then

$$P_0(t) = \frac{N_0}{N_t} = e^{-m}(e^{-k_0t} - 1) + e^{-m}e^{me^{-kt}} \quad (11)$$

where  $m$  is the arithmetic average number of impurities per droplet,  $k_0$  is the homogeneous nucleation rate, and  $k$  is the heterogeneous nucleation rate for a single impurity per drop. Equation 11 was applied to eflucimibe nucleation experimental data, and the results are presented in Figure 9. The data are well fitted by this equation, and the kinetic constants obtained are given in Table 4. The order of magnitude of the homogeneous nucleation rate obtained in this study ( $J_0 \approx 0.205 \text{ cm}^{-3} \cdot \text{s}^{-1}$ ) is in good agreement with the one obtained in a previous study<sup>16</sup> ( $J_0 \approx 0.4 \text{ cm}^{-3} \cdot \text{s}^{-1}$ ) for the same supersaturation ratio.

Based on this model, this approach allows the determination of heterogeneous and homogeneous nucleation rates in a single experiment. At low time scales, eflucimibe in droplets containing active centers (impurities) would crystallize first and thus yield a rapid initial rate (i.e., the first part of the curve in Figure 9, corresponding to the heterogeneous nucleation rate  $k$ ). At higher time scales, once all the droplets containing impurities have

**Table 4. Nucleation Kinetic Parameters of Eflucimibe (from eq 11)**

$m$	$k_0 \text{ (s}^{-1}\text{)}$	$k \text{ (s}^{-1}\text{)}$
0.16	$1.23 \times 10^{-6}$	$4.24 \times 10^{-4}$

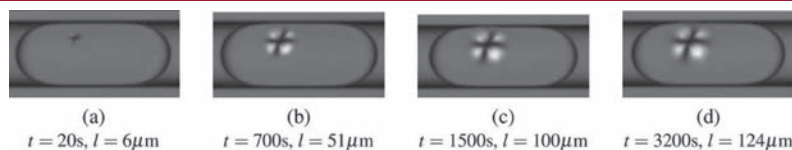


**Figure 11.** Growth of eflucimibe crystal at  $T = 20 \text{ }^\circ\text{C}$ .

crystallized, leaving only the droplets that are free of impurities, the rate would fall off (i.e., the second part of the curve in Figure 9), which allows to determine the homogeneous nucleation rate ( $k_0$ ).

*Eflucimibe Crystal Growth.* Once a crystal is formed in a droplet, it is also possible to isolate droplets for measuring the crystal growth rate as a function of time. For instance, photographs of a growing eflucimibe crystal in a droplet as a function of time are given in Figure 11.

The evolution of the radius of spherulitic crystals, obtained in 11 randomly chosen droplets, as a function of time is plotted in Figure 12. This figure clearly shows that once the crystal is formed, it grows at the same rate in these droplets. In addition, the radius scales with time as  $t^{1/2}$ , characteristic of diffusion-controlled growth.<sup>21</sup>

The spherulitic shape of the crystals obtained suggests that they are type 1 spherulites, which is assumed to be a result of heterogeneous nucleation, with thin needles radially growing outward from a heterogeneity (foreign particle or liquid droplet).

*Phase Transition of Ibuprofen.* The spherical crystallization process may be used to produce spherical agglomerates of fine crystals. This process involves the formation of a quasi-emulsion (an emulsion with a short lifetime) of a solution of solute and a good solvent in a nonsolvent. Crystallization occurs by counter-diffusion of poor solvent and good solvent. In a previous study,<sup>22</sup> this process, carried out in stirred reactors, was applied to the crystallization of ibuprofen in several organic solvents in pure water or in a mixture of water and poly(vinyl acrylate) (PVA). Depending on the process operating conditions and on the physicochemical properties of the solvent used, the authors showed that different crystals or agglomerates shapes are obtained. In particular, when no surfactant is added to water, the almost-spherical particles obtained are not the result of an agglomeration process of tiny crystals inside the droplet but

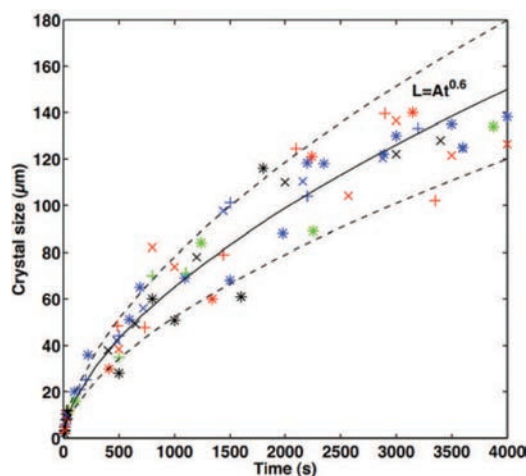


**Figure 12.** Evolution of radius of spherulitic crystals, obtained in different droplets, as a function of time.

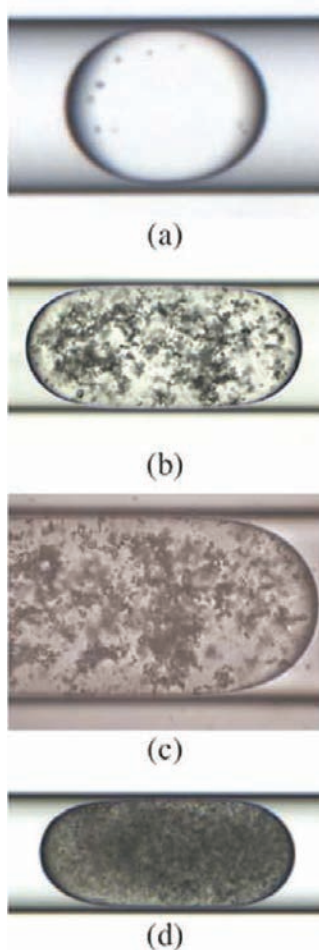


**Figure 13.** Liquid–liquid phase separation of ibuprofen in ethyl acetate droplets: (a) droplet nucleation; (b, c) after 1 min; (d) gel-like particle after 1 week.

rather the result of spherulitic crystal growth. However, the origin of this spherulitic growth is still unknown (impurities or droplet from a liquid–liquid phase separation).

To get some information on the phase transition in a single droplet, the same experiments were performed in the microfluidic crystallizer. Several solvents (ethyl acetate, methyl ethyl ketone, and octanol) were used, and supersaturation was created either by a thermal gradient (by cooling the moving droplet from 45 to 20 or to 5 °C) or by mass transfer (mainly due to diffusion of the organic solvent out of the droplet into water) or both.

During these experiments, it was observed that ibuprofen did not crystallize in the droplets for any of the operating conditions explored in this study. Indeed, as shown in Figure 13, the system undergoes a liquid–liquid phase separation (LLPS) instead of a crystallization. When the solution is kept at 20 °C, the obtained liquid–liquid system has a long lifetime. This phenomenon has already been observed for ibuprofen in pure ethanol and ethanol/water mixtures by He et al.<sup>23,24</sup> in a classical crystallization apparatus. In these work, the authors suggest that the arrest of crystal nucleation in ibuprofen solutions could be due to low crystal nucleation kinetics but also to a change of the solution medium, such as viscosity. In addition, when the obtained metastable liquid system is cooled from 20 to 5 °C, the system evolves to a gel-like

structure, as shown in Figure 13d. Similar results have been observed with other druglike molecules. At the moment, there is no explanation for this type of LLPS that does not promote nucleation.

## ■ CONCLUSIONS

In this work, a microfluidic device for investigating nucleation rate, growth kinetics, and phase transition of organic crystals in organic solvents was developed. This setup allows storage of up to 2000 small crystallization containers, with volumes ranging from 20 to 100 nL, and to control precisely their temperature and concentration. It is shown that this system is suitable to study nucleation and phase transitions of organic crystals in organic solvents. For eflucimibe crystallization, the microfluidic device enabled us to show that nucleation is due at lower time scales to a heterogeneous nucleation mechanism at the liquid–liquid interface and at higher time scales to a homogeneous nucleation process. The experimental data obtained are well described by the heterogeneous nucleation model developed by Pound and La Mer. To state whether it is impurities or the presence of the interface itself that catalyzes nucleation, we are currently performing nucleation studies by adding additives to water or to the organic solvent to change the interfacial energy.

For ibuprofen, due to the low crystal nucleation kinetics, the system undergoes a liquid–liquid phase separation for all the solvents and operating conditions tested. In that case, the developed microfluidic device is a new experimental technique for studying phase diagrams and the metastable states of small organic molecules in organic solvents.

We believe that this system will give us new opportunities to study nucleation and phase transitions of complex materials.

## ■ AUTHOR INFORMATION

### Corresponding Author

\*E-mail Sebastien.Teychene@ensiacet.fr.

## ■ ACKNOWLEDGMENT

We acknowledge the ANR (Microcrystal Project 06-BLAN-0355) and CNRS for supporting this study.

## ■ REFERENCES

- (1) Turnbull, D.; Vonnegut, B. *Ind. Eng. Chem.* **1952**, *44*, 1292–1298.
- (2) Pound, G. M.; La Mer, V. K. *J. Am. Chem. Soc.* **1952**, *74*, 2323–2332.
- (3) Knezic, D.; Zaccaro, J.; Myerson, A. S. *J. Phys. Chem. B* **2004**, *108*, 10672–10677.
- (4) Zheng, B.; Tice, J. D.; Roach, L. S.; Ismagilov, R. F. *Angew. Chem.* **2004**, *116*, 2562–2565.
- (5) Zheng, B.; Roach, L. S.; Ismagilov, R. F. *J. Am. Chem. Soc.* **2003**, *125*, 11170–11171.
- (6) Gerdtts, C. J.; Tereshko, V.; Yadav, M. K.; Dementieva, I.; Collart, F.; Joachimiak, A.; Stevens, R. C.; Kuhn, P.; Kossiakoff, A.; Ismagilov, R. F. *Angew. Chem., Int. Ed.* **2006**, *45*, 8156–8160.
- (7) Lee, J. N.; Park, C.; Whitesides, G. M. *Anal. Chem.* **2003**, *75*, 6544–6554.
- (8) Laval, P.; Salmon, J.-B.; Joanicot, M. *J. Cryst. Growth* **2007**, *303*, 622–628.
- (9) Laval, P.; Lisai, N.; Salmon, J.-B.; Joanicot, M. *Lab Chip* **2007**, *7*, 829–834.
- (10) Dombrowski, R. D.; Litster, J. D.; Wagner, N. J.; He, Y. *Chem. Eng. Sci.* **2007**, *62*, 4802–4810.

- (11) Goh, L.; Chen, K.; Bhamidi, V.; He, G.; Kee, N. C. S.; Kenis, P. J. A.; Zukoski, C. F.; Braatz, R. D. *Cryst. Growth Des.* **2010**, *10*, 2515–2521.
- (12) Wasai, K.; Kaptay, G.; Mukai, K.; Shinozaki, N. *Fluid Phase Equilib.* **2007**, *254*, 67–74.
- (13) Reguera, D.; Bowles, R. K.; Djikaev, Y.; Reiss, H. *J. Chem. Phys.* **2003**, *118*, 340–353.
- (14) Grossier, R.; Veessler, S. *Cryst. Growth Des.* **2009**, *9*, 1917–1922.
- (15) Teychene, S.; Autret, J.; Biscans, B. *J. Pharm. Sci.* **2006**, *95*, 871–882.
- (16) Teychene, S.; Biscans, B. *Cryst. Growth Des.* **2008**, *8*, 1133–1139.
- (17) Teychene, S.; Autret, J. M.; Biscans, B. *Cryst. Growth Des.* **2004**, *4*, 971–977.
- (18) Teychene, S.; Autret, J. M.; Biscans, B. *Chem. Eng. Technol.* **2006**, *29*, 251–256.
- (19) Izmailov, A. F.; Myerson, A. S.; Arnold, S. J. *Cryst. Growth* **1999**, *196*, 234–242.
- (20) Dombrowski, R. D.; Litster, J. D.; Wagner, N. J.; He, Y. *AIChE J.* **2010**, *56*, 79–91.
- (21) Granasy, L.; Pusztai, T.; Tegze, G.; Warren, J. A.; Douglas, J. F. *Phys. Rev. E* **2005**, *72*, No. 011605.
- (22) Teychene, S.; Sicre, N.; Biscans, B. *Chem. Eng. Res. Des.* **2010**, *88*, 1631–1638.
- (23) He, G.; Tan, R. B. H.; Kenis, P. J. A.; Zukoski, C. F. *J. Phys. Chem. B* **2007**, *111*, 14121–14129.
- (24) He, G.; Tan, R. B. H.; Kenis, P. J. A.; Zukoski, C. F. *J. Phys. Chem. B* **2007**, *111*, 12494–12499.